Global Journal of Researches in Engineering: D
Aerospace Science
Volume 22 Issue 1 Version 1.0 Year 2022
Type: Double Blind Peer Reviewed International Research Journal
Publisher: Global Journals
Online ISSN: 2249-4596 & Print ISSN: 0975-5861

Experimental Ablation Measurements in Hypersonic Flows using Novel Preheating Technology

By Daniel Odion Iyinomen

Abstract- Measurements of mass ablation rates in hypersonic flows are used to calibrate computational models, and the arc jets have been the norm for ablation experiments. However, the quality of experimental data from arc jet facilities are limited by non-uniform enthalpy distribution, non-equilibrium state, change of surface quality during testing, and the extent of oxidation. This publication presents an innovative research work, leading to a new era of scientific breakthrough in aerothermodynamics experiments and hypersonic re-entry studies using new preheating technology. The impetus for this new technology is to help reduce the large variations in ablation rate predictions around the world. A graphite disc of 50 mm diameter and 2 mm thickness was heated from the downstream side with a plasma to approximately 2500 K, and then exposed to a cold Mach 4.5 flow using the Ludwieg tube facility at the University of Southern Queensland (TUSQ) in the atmospheric blowdown configuration. The experimental probe was very similar to the European standard probe, and presented herein are the results from material loss and surface recession for the experiments. The next generation experimental model (NGEM), which has been specifically designed for the next generation of researchers is also presented, to be used in validating computational models in excess of 3000K surface temperatures under conditions that replicate characteristics of re-entry flights.

GJRE-D Classification: *FOR Code: 090199*

Strictly as per the compliance and regulations of:

Experimental Ablation Measurements in Hypersonic Flows using Novel Preheating Technology

Daniel Odion Iyinomen

Abstract- Measurements of mass ablation rates in hypersonic flows are used to calibrate computational models, and the arc jets have been the norm for ablation experiments. However, the quality of experimental data from arc jet facilities are limited by non-uniform enthalpy distribution, non-equilibrium state, change of surface quality during testing, and the extent of oxidation. This publication presents an innovative research work, leading to a new era of scientific breakthrough in aerothermodynamics experiments and hypersonic re-entry studies using new preheating technology. The impetus for this new technology is to help reduce the large variations in ablation rate predictions around the world. A graphite disc of 50 mm diameter and 2 mm thickness was heated from the downstream side with a plasma to approximately 2500 K, and then exposed to a cold Mach 4.5 flow using the Ludwieg tube facility at the University of Southern Queensland (TUSQ) in the atmospheric blowdown configuration. The experimental probe was very similar to the European standard probe, and presented herein are the results from material loss and surface recession for the experiments. The next generation experimental model (NGEM), which has been specifically designed for the next generation of researchers is also presented, to be used in validating computational models in excess of 3000K surface temperatures under conditions that replicate characteristics of re-entry flights.

I. Introduction

The dominance of aerodynamic heating in hypersonic flight regime [Tranet al. 2006] is the most critical factor that drives the principal design characteristics of any re-entry vehicle [Goulard 1958]. Methodologies for aerodynamic heat estimations range from simple to complex, depending on the required amount of time and computational resources [Poovathingalet al. 2016]. The maximum heat flux for a blunt-body can be assumed to occur at the stagnation point [Duffa2013], though there are some few exceptional cases. Fay and Riddle originally investigated stagnation point heating problem in the 1950s [Fay and Riddell 1958], then further investigated for re-entry applications by Allen and Eggers [Julian and Eggers 1958], and by Sutton and Graves during the Apollo era for different gas mixtures [Sutton and Graves 1971]. A very simplified expression for estimating the hypersonic aerodynamic heating was proposed by Sutton and Graves as stated in Eq. (1).

$$Q_{Conv} = 1.73 \times 10^{-4} \left[\frac{\rho_\infty}{R_n}\right]^{0.5} V_\infty^3 \qquad \text{Eq. (1)}$$

where, Q_{Conv} is convective heat flux (W/m2), ρ_∞ is free stream density (kg/m3), R_n is nose radius of body (m), V_∞ is free stream velocity (m/s). A similar relation for a preliminary analysis of the stagnation point heat transfer was also proposed by Detra and Hidalgo [Detra and Hidalgo 1961] as stated in Eq. (2).

$$Q_{Conv} = 5.16 \times 10^{-5} \left[\frac{\rho_\infty}{R_n}\right]^{0.5} V_\infty^{3.15} \qquad \text{Eq. (2)}$$

Some mathematical modifications were later proposed by Tuber (1989) by addressing the enthalpy at the edge of boundary layer (h_w) and total enthalpy at the stagnation point (h_o) [Tauber 1989] as stated in Eq. (3).

$$Q_{Conv} = 1.83 \times 10^{-4} \left[\frac{\rho_\infty}{R_n}\right]^{0.5} V_\infty^3 \left[1 - \frac{h_w}{h_o}\right] \qquad \text{Eq. (3)}$$

The above-mentioned equations explain why windward-facing surface of a re-entry vehicle is always kept blunt because the heating varies directly with the cube of velocity and inversely with the square root of the nose radius [Chhunchha 2018]. However, these empirical formulations were reasonable approximations that do not characterize the exact solution. Goulard reported that the validity of Lees, Fay and Ridell heat transfer solutions are shown to correspond to the limiting case of an infinitely fast catalyst; and extended the solutions to the general case of a wall offinite catalytic efficiency, by introducing a correction factor [Goulard1958]. The more exact numerical results of Fay and Riddell, are correlated as (1) equilibrium boundary layer, (2) frozen boundary layer with an equilibrium catalytic wall, and (3) frozen boundary layer with a noncatalytic wall [Anderson 2000]. For equilibrium boundary layer (spherical nose), the surface heat transfer (Q_w) is given as Eq. (4).

Author: B.Eng. (Hons), MSc, PhD- Mechanical & Aerospace Engineering. Hypersonic Re-entry Specialist, Aerospace Research & Innovations, Danospace Intelligence Worldwide.
e-mail: iyidaniel@yahoo.co.uk

$$Q_w = 0.76Pr^{-0.6}[\rho_e\mu_e]^{0.4}[\rho_w\mu_w]^{0.1}\sqrt{\left(\frac{du_e}{dx}\right)_s}\left(h_{0_e} - h_w\right) \times \left[1 + \left(Le^{0.52} - 1\right)\left(\frac{h_D}{h_{0_e}}\right)\right] \quad \text{Eq. (4)}$$

where ρ is the mass density, μ is the absolute viscosity, $\frac{du_e}{dx}$ is the velocity gradient, h is the enthalpy per unit mass, Pr is the Prandtl number and the subscripts *0*, *e* and *w* describe the total, the conditions at the edge of the boundary layer edge and at the wall, respectively. Le is the Lewis number, h_D is the dissociation enthalpy which is expressed as the product of the enthalpy of formation $\Delta h^0_{F,i}$ of species i and its mass fraction y_i stated in Eq. (5).

$$h_D = \sum_{i=1}^{N} y_i \Delta h^0_{F,i} \quad \text{Eq. (5)}$$

For frozen boundary layer with an equilibrium catalytic wall (spherical nose) the surface heat transfer (Q_w) is stated in Eq. (6).

$$Q_w = 0.76Pr^{-0.6}[\rho_e\mu_e]^{0.4}[\rho_w\mu_w]^{0.1}\sqrt{\left(\frac{du_e}{dx}\right)_s}\left(h_{0_e} - h_w\right) \times \left[1 + \left(Le^{0.63} - 1\right)\left(\frac{h_D}{h_{0_e}}\right)\right] \quad \text{Eq. (6)}$$

For frozen boundary layer with a noncatalytic wall (spherical nose), the surface heat transfer (Q_w) is stated in Eq. (7). It is generally believed that for frozen flow profile, the atomic mass fraction between the wall and the outer edge is not as a result of any chemical reactions within the boundary layer, but rather is completely as a result of diffusion of the atoms from the outer edge to the wall [Anderson 2000].

$$Q_w = 0.76Pr^{-0.6}[\rho_e\mu_e]^{0.4}[\rho_w\mu_w]^{0.1}\sqrt{\left(\frac{du_e}{dx}\right)_s} \times \left[1 - \left(\frac{h_D}{h_{0_e}}\right)\right] \quad \text{Eq. (7)}$$

The velocity gradient $\frac{du_e}{dx}$ can be represented by β, the total enthalpy h_0 and the chemical compositionat the boundary layer edge contained in the h_{D_e} term, including the wall conditions of enthalpy and catalycity can then be treated as duplication parameters [Sakrakeret al. 2021]. The exponent of Lewis number, *Le*, in Eq. (4) is given as 0.52 for an equilibrium boundary layer and 0.63 for a frozen boundary layer with fully catalytic wall; wherein the latter is suggested as 2/3 by Lees [Lees 1956]. Due to the crucial nature of stagnation heating and the boundary layer chemistry in hypersonic entries, it is very important to reproduce the flight conditions in ground test facilities as accurately as possible. Figure 1 presents the summary of recombination rate parameter for various wall conditions.

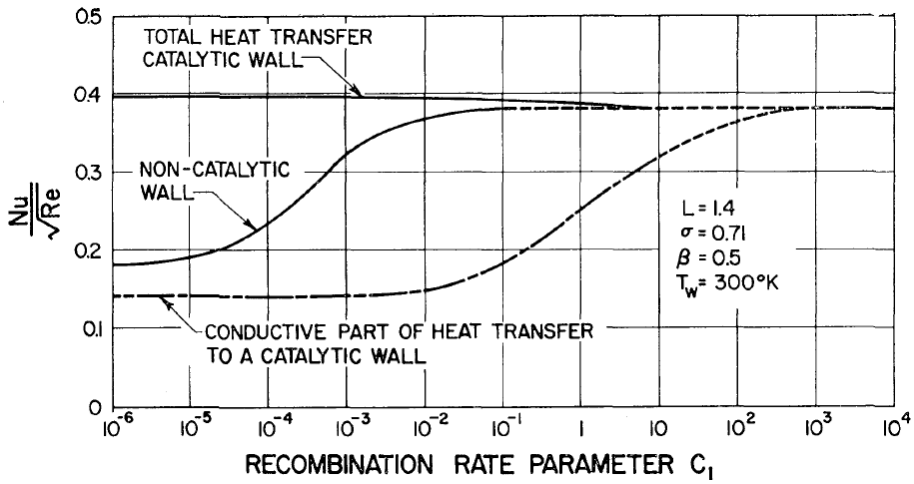

Figure 1: Summary of recombination rate parameter for various wall conditions [Fay and Riddell 1958].

In high-enthalpy facilities, the gas is either partially or totally dissociated before reaching the surface. Using such facilities for Martian re-entry studies, carbon dioxide molecules do not get to the surface because they start to dissociate inside the arc chamber, thus, having some consequences on the nozzle flow and quality of experimental data. In addition, the use of a gas different from air, such as a CO_2 environment, has a strong impact on the arc chamber and notably on the arc performance in most high-enthalpy facilities [Bugel et at 2011]. In the present work, these high-enthalpy problems are completely eliminated and the surface temperature is completely responsible for the actual dissociation and recombination of gas species. The rationale behind this innovation is to achieve an alternative thermal coupling of gas–surface interactions with a high degree of confidence [Iyinomen 2022a]. The credibility demonstrated for extreme re-entry problems makes the present work an indispensable tool for re-entry aerothermodynamics studies. The inherent

advantages that are associated with the novel plasma preheating technology presented herein include but not limited to (1) light weight and portability of model, (2) surface temperature control to replicate re-entries, (3) excellent temperature profile across the surface of sample, (4) capability to replicate entries for different planetary missions due to its ability to perform well in all types of re-entry gases like O_2 N_2, Air, CO_2, He, Ne, Ar, H_2, CH_4, NH_3, etc., (5) capability to experiment different types of heatshield materials like PICA, SIRCA, Avecoats, C/C composites, and graphite to name a few, (6) capability to experiment different axisymmetric probe geometries not limited to Stardust, Orion, Hayabusa, and SpaceX-dragon, (7) capability to perform well in both short and long duration wind tunnel facilities,(8) the technique inherently eliminates arc chamber problems that are associated with most high-enthalpy facilities, (9) the technique inherently produces much lower greenhouse emissions, and (10) the technique is inherently economical and less than 10% of the operational costs of running the high-enthalpy plasmatrons and NASA Ames arcjet facilities.

II. Overview

Reliable heat-shielding is essential, physical re-entry processes are complicated, experiments are needed to support model development, and hypersonic impulse facilities cannot perform ablation tasks if cold-walled [Iyinomen at al 2021]. The aim of this present work is to quantitatively measure the ablation and oxidation rates in a hypersonic boundary layer using a new hot-surface plasma preheating technology to heat to the required surface temperatures for re-entry studies in a hypersonic impulse facility. This is a new experimental method for heating material samples using a high temperature plasma arc fixture. This new fixture was integrated within a cold flow Mach 4.5 wind tunnel in order to measure material ablation and mass loss due to aerodynamic flow effects. This work provides details of the experimental method, few CFD simulation results in support of the experiments, and a series of mass loss measurements and microscopic images to quantitatively and qualitatively observe material mass loss and surface modifications. A temperature of 2500K was achieved in the test specimen [Iyinomen 2020a]. The surface temperature measurements, uncertainty in measurements, temperature variation from stagnation point to the edges (shoulders),and percentage (%) deformation of material sample after test had earlier been published extensively by the author [Iyinomen et al. 2021] and will not be repeated here. The radial temperature distribution along the surface is also available elsewhere [Iyinomen 2022a]. Details on the numerical method, grid, boundary conditions, probe axis along the axisymmetric centre-line (stagnation-line) of the flow, shock resolution, source of the carbon species, surface chemistry/ablation model adopted, the presence of carbon species so far removed from the face of the probe, the unit Reynolds number for the flow conditions, and the motivation for using the same graphite disc for all the final heating runs had already been made available by the author [Iyinomen 2020b].

This work creates a genuinely interesting approach to probing high temperature effects in a cold flow tunnel and documentation of mass loss from their specimens using dimensional values. The quantifiable measurements of mass loss can then be connected to ablation theory or models. The measurement techniques mostly focus on mass loss and recession of the tested graphite disc, applying tools such as the Romer Multi-Gage 6-axis Coordinate Measuring Arm, the laser beam technique, and the Scanning Electron Microscope (SEM) were used to obtain experimental data with focus on ground-based characterisation techniques for thermal protection material analysis. The topic treated in this manuscript is of importance to the international research community, especially in the field of new ground-testing facilities for ablation analysis and in the context of material response model validation. The author is highly pleased to present a new test facility and new measurement technique for the acquisition of data for model calibration/validation. Apparatus development for the new preheating methodology, calibration of camera and spectrometer, and FEA simulations have shown that the determined temperature profile of the heated disc is suitable to continue with mass loss assessments [Iyinomen 2020b, Iyinomen et al. 2021].

Recent experiments based on Orion re-entry conditions used a surface temperature of about 2800 K [Glass 2008] and Apollo 4 lunar return speed of 11 km/s reportedly experienced a surface temperature of about 2400 K [Decand Braun2006], while typical re-entry surface temperatures for Space Shuttles was about 1740 K [Glass 2008]. This present work has achieved temperatures in excess of 2500 K on a preheated graphite surface used for the assessment of mass loss through ablation in a Mach 4.5 flow. The use of a plasma as the means of heating the disc was proven to be effective for reaching temperatures of these magnitudes and the process has potential to be more widely used for similar experiments [Iyinomen 2022a]. This work reports the first-time quantification of ablation and oxidation rates of a heated carbon disc in a Mach 4.5 flow up to 500 milliseconds duration in a hypersonic wind tunnel facility using the preheating methodology [Iyinomen 2019]. Two methods were utilised in the ablation measurements which will be discussed in Section V: (1) weighing method, and (2) volume-based method. The model in the present work can be likened to the European standard probe [Fagnaniet al.2019] positioned at a zero-degree angle of attack to the incoming flow [Zhanget al. 2019], and heated from the

downstream side using a plasma to temperatures in excess of 2500K. The separation of the tungsten electrode from the disc surface and the length that the electrode protruded from the shroud had significant effects on the ability to start a plasma. Preheating of the graphite disc was achieved with plasma [Wang et al. 2019, Traidia 2011] generated by a DC current [Siewert et al. 2019, Anand et al. 2017] between a tungsten electrode and the back (downstream) side of the disc. Figure 2 is a sectional view of the model which illustrates the Thermophysics and heat transfer processes from the hot plasma to the disc. The power generating technique is shown in Figure 3.

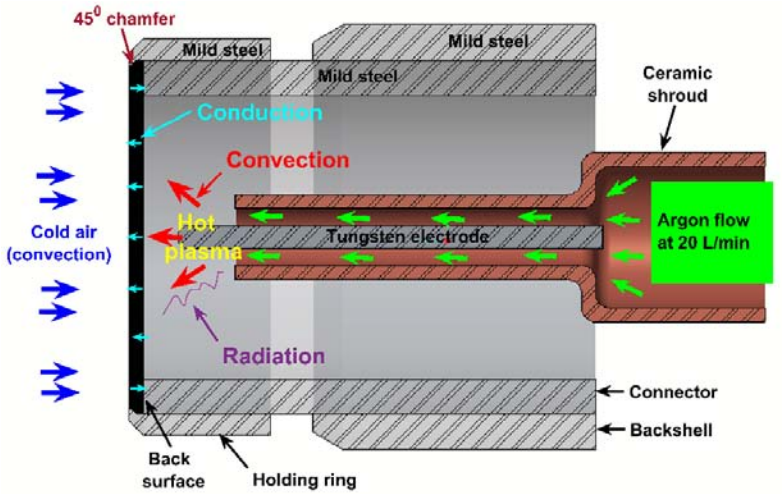

Figure 2: The new plasma preheating technique illustrating the Thermophysics and heat transfer processes from hot plasma tographite disc [Iyinomen 2020a].

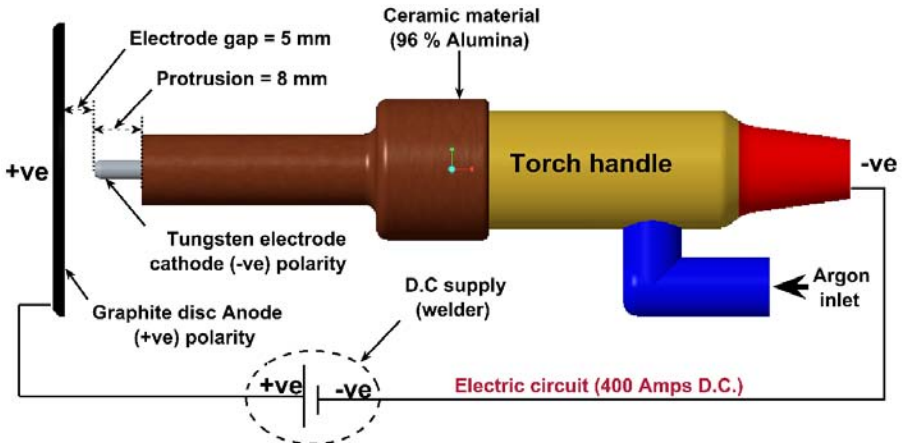

Figure 3: Illustrating electrical heat generation at 400A power rating [Iyinomen 2020b].

The two most critical geometric parameters controlling the heat flux to the workpiece (graphite) are electrodegap and protrusion. The orientation of the tungsten inert gas (TIG) torch is centralised in the model to enable even thermal spread from the centre to the edges. This made it possible for the probe model to assume an axisymmetric orientation. Experimental heating conducted in 500 Pa vacuum pressure, for 15 seconds using the plasma preheating technology is illustrated in Figure4 to preheat model to the desired temperatures (about 2500 K) just before the flow starts. The data from temperature measurements were extracted through the fibre optics.

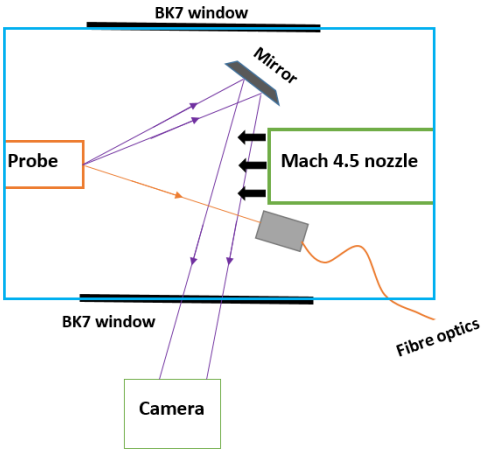

Figure 4: Schematic layout of setups for ablation experiments. Temperature data was made available via fibre optics and connected to the data acquisition system for data extraction and processing [Iyinomen et al. 2021].

III. Methodology

An accurate assessment of the duration of the flow in the experiments is essential for accurate evaluation of the mass loss rate. The TUSQ data acquisition system (DAQ), automatically saves the run times which allows the duration of each run to be determined [Birch et al. 2018]. Confirmation of the flow characteristic of the nozzle (nozzle start) was supported by Schlieren high-speed video images [Settles 2006]. Knowing the mass losses and using the run times from the DAQ, the average material loss rate was determined. For each of these sets of runs, the total duration and total mass loss were used to determine the mass loss rates. The Schlieren images in Figure 5 show the orientation of the experimental modelrelative to the pressure survey system, which was used to characterise the flow properties. The Schlieren images forthe three classes of tests (flow-only case, heated-only case, and heated-with-flow case) were used in the present work.

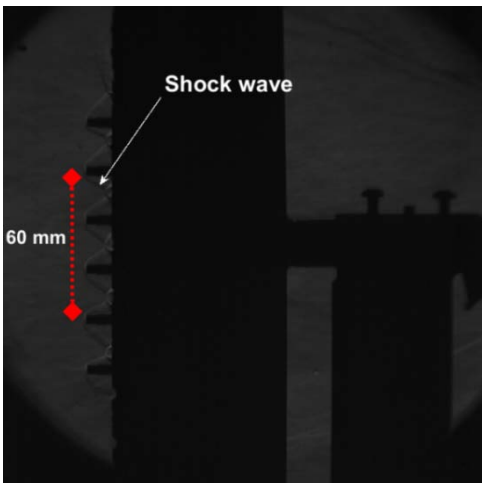

(a) Pressure survey array at Mach 4.5.

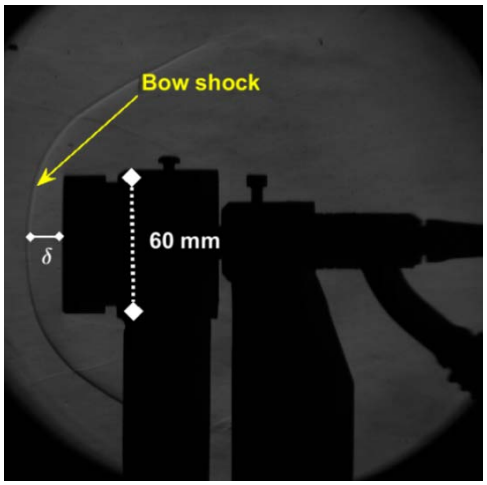

(b) Flow-only case at Mach 4.5.

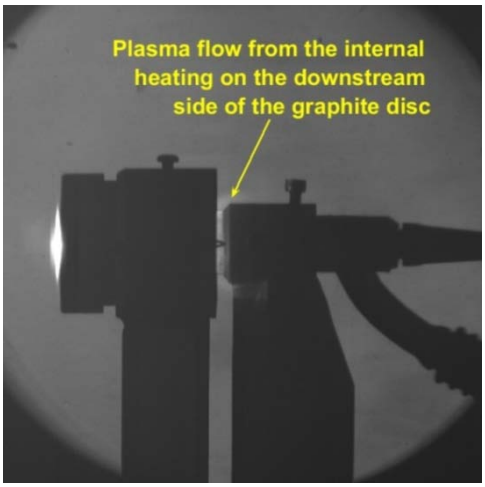

(c) Heated-only case at 2500K.

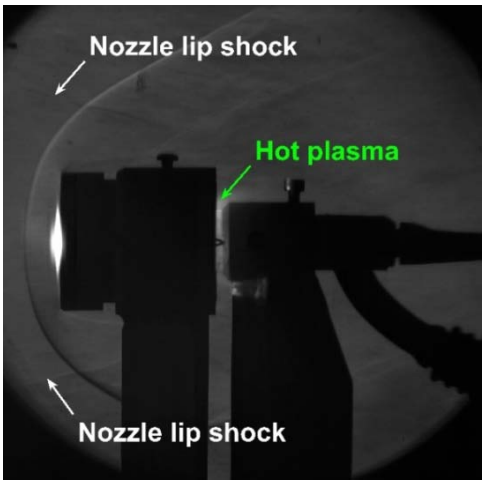

(d) Heated-with-flow case at 2500K and Mach 4.5.

Figure 5: High-speed camera Schlieren imaging was used for aerodynamic validations, where the heated-only case was taken at about the time flow would normally starts [Iyinomen 2019].

1. *Flow-Only Case:* The disc used in the flow-only case was placed in the holding ring. The test section was sealed and the vacuum pump operated for approximately 20 minutes to reduce the test section pressure to approximately 500 Pa. No preheating was applied before the main valve was operated to produce the flow. Flow durations were typically 0.5 seconds.
2. *Heated-Only Case:* The disc holder surfaces were cleaned and the disc installed. A new electrode was placed in the TIG torch and the TIG settings required for the plasma were applied. The test section was sealed and vacuum pumps operated and after the 20 minutes required to reduce the test section pressure to approximately 500 Pa, the run was commenced by initiating the plasma. The plasma heated the disc for 15 seconds, manually timed. No flow was used in this case.
3. *Heated-With-Flow Case:* The disc was set up and heated for 15 seconds as per heated-only case. The flow was initiated after 15 seconds of heating, manually timed. The heating remained on during the entire flow duration of about 0.5 seconds. The Schlieren technique based on the principle of changing densities in the gas was used to identify the establishment of the bow shock and therefore the commencement of Mach 4.5 flow. The high-speed camera was set at a frame-rate of 2500 fps and frames at the specific points during the flow are shown in Figures 6 and 7.

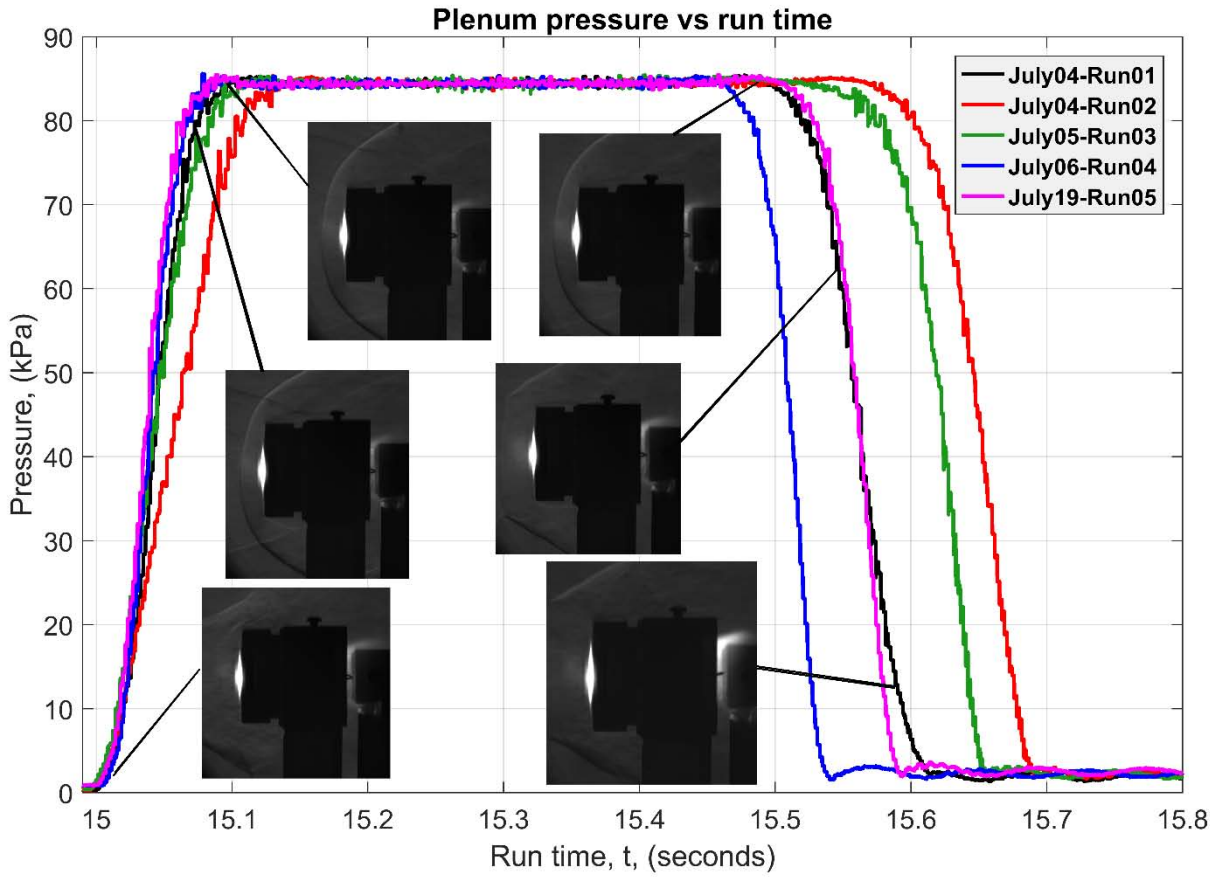

Figure 6: Matching run times with Schlieren images to identify when flow starts [Iyinomen 2020a].

The start and end times for the sixteen (16) heated-with-flow runs for the second phase of the experiments are shown in Figure 7. The shortest run time was 0.45 seconds while the longest was 0.64 seconds. This gives an average run time of 0.54 seconds for a 16 heated-with-flow run.

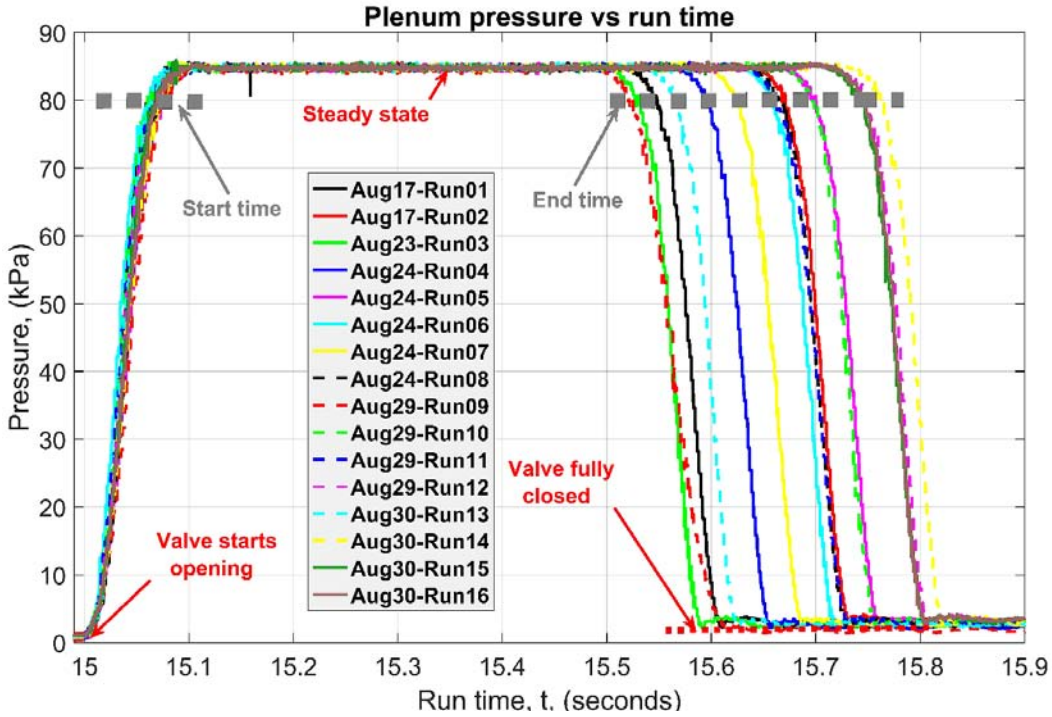

Figure 7: The start and end times from the 16 heated-with-flow run of the experiments used to determine material loss rates. Mass loss was measured for each of runs 1 and 2, then at the end of runs 4, 8, 12 and 16 [Iyinomen 2020a].

Analytical methods were used to estimate the power requirements for preheating the samples. The result from analytical methods was compared with the calibrated data from previous work as shown in Figure 8. The current ranged from zero to 700 Amps because the maximum output from the welding machine was 700 Amps at the time of experiments. The heating starts from ambient temperature and the poly-fit was obtained by applying the Least square fitting for second-order polynomials to the calibrated temperature data at 200, 250, 300, 350, and 400 Amps. Figure 8 shows that the calibrated surface temperatures have good agreements with the estimated surface temperatures.

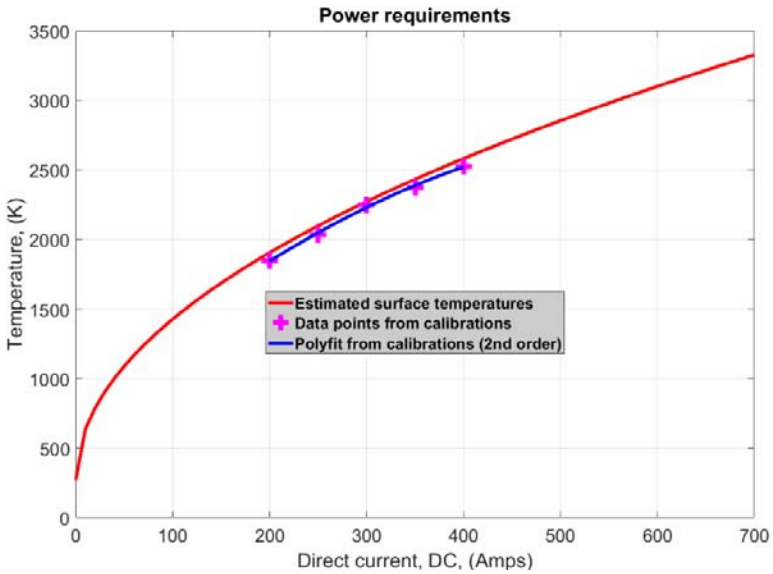

Figure 8: Power requirements for preheating ablation samples [Iyinomen 2022a].

IV. Flow Properties and Species Transports

Flow properties associated with the present work were obtained from CFD simulations using ANSYS Fluent. Surface temperatures and boundary conditions in the CFD were set using measurement information from experiments. Figure 9 indicates that the temperature has not changed significantly until within 1 mm from the wall, so the concentration of products was not entirely driven by temperature alone.

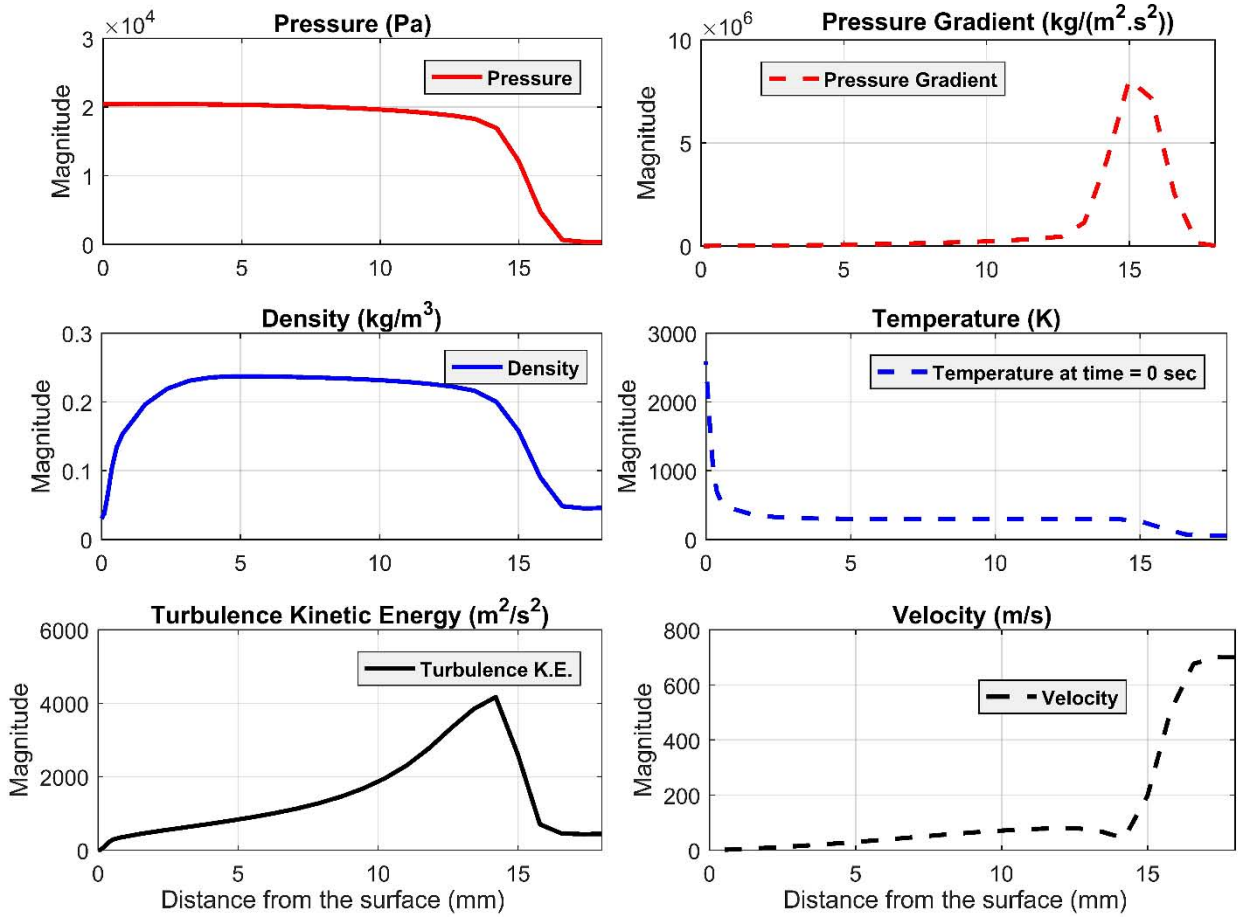

Figure 9: Flow properties along the probe axis stagnation line from CFD simulations [Iyinomen 2020b].

Species transports are driven by flow properties. Thermally initiated chemical reactions are the formation process of all carbonaceous species in Figure 10 except for the carbon sublimation species, C, C_2, C_3. The CO_2 species are formed from further oxidation of CO species, thus making CO_2 a secondary reaction. The CO_2 concentration shows a maximum at the stagnation flow region where the O species are maximum, which suggests the requirement of O species for CO_2 formation. The result also shows that CO_2 has a sharp drop from the peak value to almost zero at the surface within the experimental temperature limit of 2530 K. The CN species distribution also shows a similar pattern to that of CO_2. This also suggests that CN is not a product of direct surface reaction within the experimental temperature limit. This further supports the absence of dissociated nitrogen atoms which would otherwise aid direct formation of CN at the surface. However, another possible path for CN production is through CO produced by the ablation reactions CO+N → CN+O [Martin at al 2010]. The sublimation species C, C_2, and C_3 were almost zero.

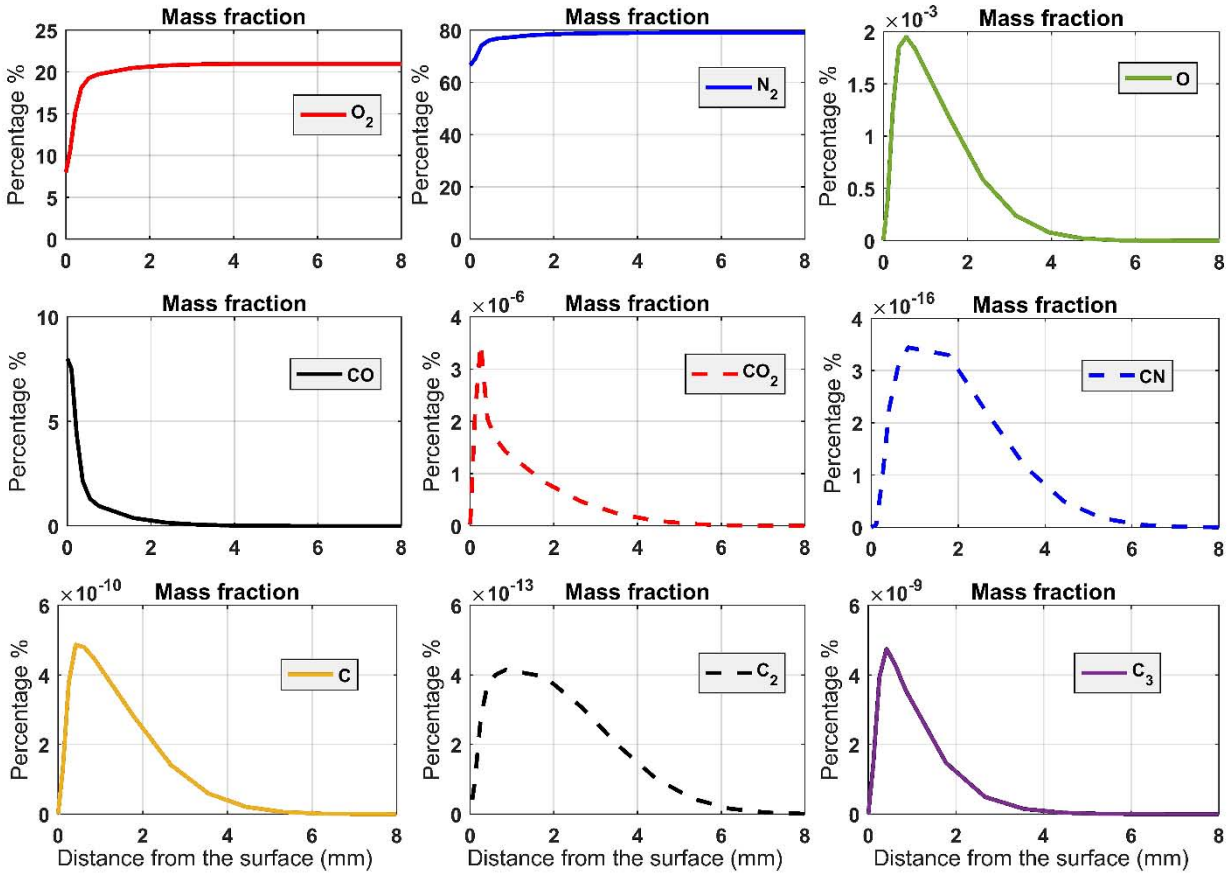

Figure 10: Species mass fractions along probe axis stagnation line- CFD simulations [Iyinomen 2020b].

The graphite ablation sample used in the present work is an iso-statically pressed graphite with grade PCC-X2 from Graphite Australia. Oxidation analysis of other materials can be made by simply reproducing the methodology and replacing the disc material properties in the simulation. The moral justification and materials properties of the graphite specimen has been published extensively by the author [Iyinomen 2020a]. Unlike the negative heat flux to the wall from the flow in high enthalpy facilities, the present work adopts a positive heat flux from the wall to the flow [Iyinomen 2022b].

V. Experimental Procedures

a) Experimental Mass Loss Measurements using Mass Weighing Method

Using the arrangement of the experiment described in Figure 5, experimental runs were conducted using three (3) different cases in two (2) phases. The first phase (phase 1) of the experiments involved different runs using random discs, while the second phase (phase 2) was more coordinated using same disc specimen throughout the sixteen (16) heated-with-flow runs. Each run required the disc to be removed for measurement and/or cleaning of the holding ring. This required the test section to be opened after each run. The experimental procedures for the final phase (phase 2) involved the following steps in a chronological sequence.

1. Graphite disc was prepared using a centre lathe by parting from a 50 mm diameter bar. Only one disc was used during the final experiments.
2. The disc was sanded by hand on emery paper against a machined flat surface to remove machining marks.
3. The disc was weighed using a mass balance.
4. The disc thickness at various positions was measured using a micrometre gauge.
5. A visualisation technique using a laser sheet produced an image representing the profile of the surface.
6. A Scanning Electron Microscope was used to show the surface texture at various positions on the disc.
7. The measured disc was subjected to one flow-only case and processes 3 to 6 were repeated.
8. The same disc was subjected to one heated-only case and processes 3 to 6 were repeated.
9. The same disc was subjected to the first of sixteen heated-with-flow runs and processes 3 to 6 were repeated.
10. The same disc was subjected to a second heated-with-flow run and processes 3 to 6 were repeated.

11. The same disc was subjected to another two heated-with-flow run after which, processes 3 to 6 were repeated.
12. The same disc was subjected to three series, each of four heated-with-flow runs and after each series, processes 3 to 6 were repeated.

To measure the degree of ablation losses, the mass loss during the experiments (flow-only, heated-only and heated-with-flow) were measured using a Kern ABT mass balance. The balance displays at an increment of 0.00001 g and reproduces a weighed mass at a resolution of 0.0001 g. The mass loss during each test was the difference in readings before and after the tests. At each weighing, the disc was placed on the balance and the machine automatically detects when the reading is stable, at which time the weight was recorded. The disc was removed from the balance, then replaced and a new weight recorded. This was repeated to record a total of three weights, which were averaged with an attributed uncertainty specified as the maximum difference between the average and any of the three recorded weights. Table 1 shows the disc mass loss for all the runs in the second phase of the experiments. Both phase 1 and phase 2 test data are presented in order to obtain a general comparison of all experimental data for same set of conditions at different times.

Table 1: Experimental data obtained from mass loss experiments from Phases 1 and 2.

Flow-only case		Heated-only case		Heated-with-flowcase	
Mass loss (g)	Run time (s)	Mass loss (g)	Run time (s)	Mass loss (g)	Run time (s)
Phase 1: Pre-test Data – several random discs were used for all three (3) cases					
0.000544	0.58	0.00816	15	0.0164	0.458
0.000475	0.51	0.00820	15	0.01735	0.480
0.000583	0.55	0.00812	15	0.01766	0.495
0.000525	0.53	0.00792	15	0.01767	0.520
0.00051	0.50	0.00803	15	0.01802	0.530
-	-	0.00806	15	0.019221	0.540
-	-	0.00810	15	0.01933	0.540
-	-	0.00799	15	0.01984	0.550
-	-	0.00802	15	0.02002	0.560
-	-	0.00830	15	0.02042	0.569
-	-	0.00822	15	0.02065	0.570
-	-	-	-	0.02083	0.580
Phase 2: Final Test Data – same disc (newly prepared) was used for all three (3) cases					
0.00050	0.495	0.00790	15	0.0138	0.450
-	-	-	-	0.0167	0.460
-	-	-	-	0.0373/ 2 runs	0.960/ 2 runs
-	-	-	-	0.0746/ 4 runs	2.200/ 4 runs
-	-	-	-	0.0811/ 4 runs	2.240/ 4 runs
-	-	-	-	0.0831/ 4 runs	2.240/ 4 runs

From Table 1, the average mass losses for flow-only, heated-only and heated-with-flow cases were 0.000527, 0.0082, and 0.0190 g respectively. The average mass loss rate, $\dot{m}_{loss}$ for the flow period of a heated-with-flow run is represented by Eq. (8), where Δm is the difference between the average mass loss from heated-only and the average mass loss from heated-with-flow runs. The parameter Δm accounts for the actual mass loss during the realflow period from the heated-with-flow runs with an average run time Δt of 0.54 seconds for this flow period. This actual mass loss during the flow period is reasonable because all heated-with-flow cases had undergone the heated-only stage before the flow was initiated.

$$\dot{m}_{loss} = \frac{\Delta m}{\Delta t} = \frac{0.0190 - 0.0082}{0.54} = 0.020\ g/s \quad \text{Eq. (8)}$$

Figure 11 presents the experimental results for the flow-only cases. The average mass loss rate for flow-only case was on average 0.0010 g/s. The mass loss itself for flow-only case was an average of 0.000527 g, which represents about 2.8% to the overall ablation for the heated-with-flow runs. It represents 4.9% of the ablation that occurs during the flow in a heated-with-flow run.

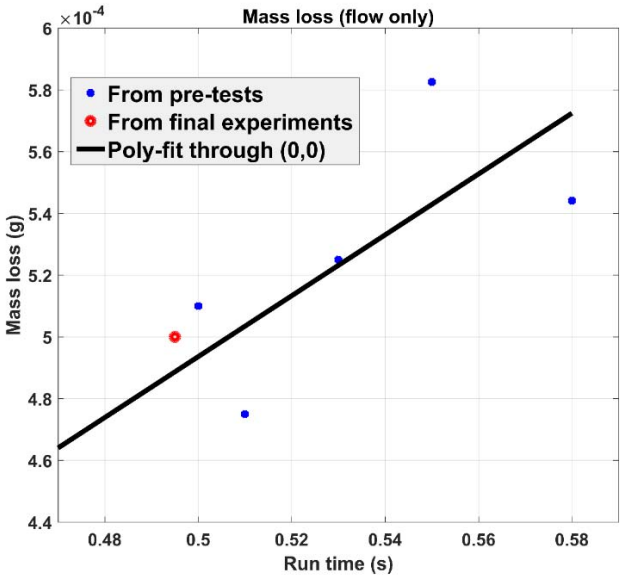

Figure 11: Plots of mass losses for flow-only cases. The datum point for the flow-only case at the start of the final 18 runs is depicted with a red-dot marker type. The mass lost rate is depicted by the slope of a linear best fit line forced through the origin, giving a mass loss rate of 0.00099 g/s.

This flow-only mass loss resulted without any chemical reactions, thus suggesting that mechanical actions were not insignificant, but only a minor contributor. For the heated-only experiments as shown in Figure 12, dividing the accumulated mass losses from the twelve different heated-only runs by the total time of heating, produces a mass loss rate. This assumes a constant mass loss rate during the heating cycle, but the temperature increased during a cycle from 0 to 15 seconds. The mass loss rate will be dependent on temperature, so a mass loss rate as a function of temperature is not obtainable from the heating only data. The average mass loss rate during a heating only run was 0.00055 g/s. A more useful value is the average mass loss per heating cycle, as the heating cycles were consistently of the same duration of 15 seconds. The average mass loss per heating cycle was 0.0082 g. The average mass loss due to the heating cycle was about 43% (0.0082/0.0190) of the overall ablation for the heated-with-flow run.

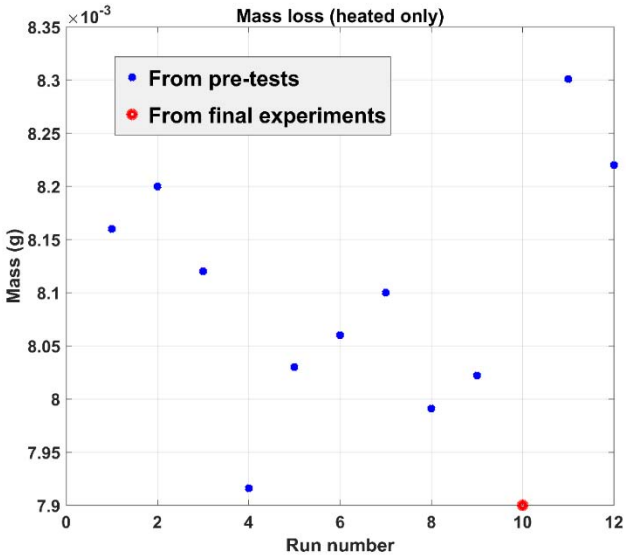

Figure 12: The results for heated-only mass loss during 15 second heating cycles.

Figure 13 shows the mass losses from sixteen heated-with-flow runs, completed at six stages (see experimental procedures 8 to 12 in Section V). The flow run time varied from 0.45 seconds to about 0.56 seconds, with a target of 0.5 seconds. The time variation was due to the manual opening and closing of the flow control valve. The mass loss shows a general increase with increasing run time. The result from step 6 shows an increase in mass loss over that of step 5 despite the same run time. This difference might be attributed to the crack, which potentially exposed more graphite material to ablation [Iyinomen 2020a], although the difference is not outside the range of the error indicated by the best fit shown in Figure 13. The red line shows the best-fit (linear fit) of which the slope is about 0.020 g/s running through point (0,0.0082), as there is already a mass loss of about 0.0082 g when the flow starts. The value 0.0082 g was obtained from the average of the heated-only experiments. It is reasonable to apply this average as the heating time was consistently the same. The

displayed flow durations for the series of heated-with-flow runs are the averages for those series.

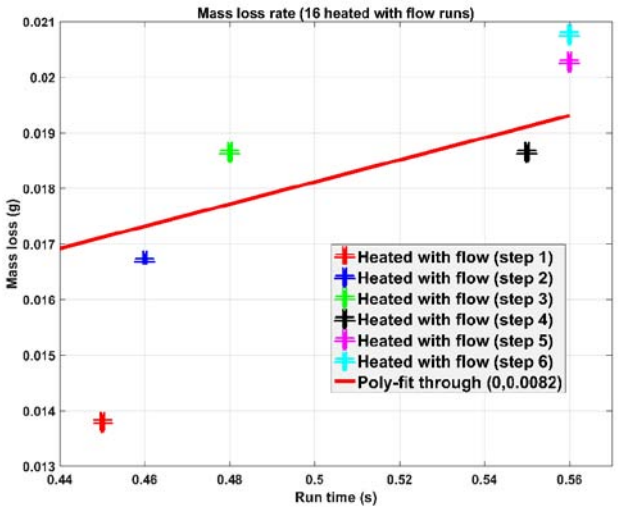

Figure 13: Result showing the mass losses for the flow period from heated-with-flow runs. The slope of the poly-fit line represents the average mass loss rate of 0.020 g/s.

As a check of the data reproducibility of the sixteen heated-with-flow runs, analysis of earlier heated-with-flow runs was carried out. Figure 14 also shows the results of the mass losses from other heated-with-flow runs from earlier experiments using pre-test data from Table 1. The mass loss rates ranged from 0.034 g/s to 0.036 g/s with an average of about 0.035 g/s. It was calculated based on the slope of a linear best fit of the plot in Figure 14, again going through the point (0,0.0082) as applied for the final 16 runs.

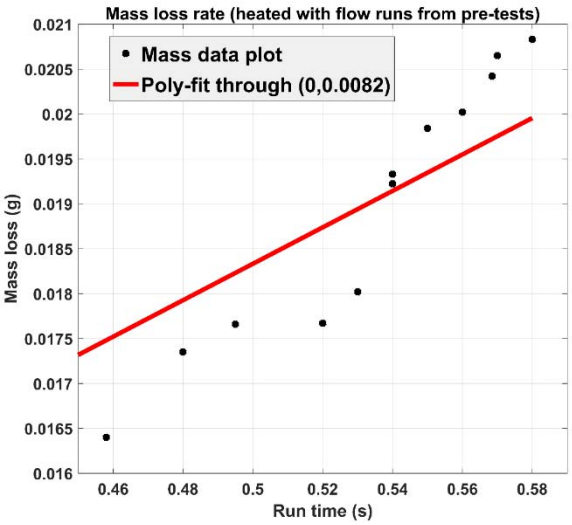

Figure 14: Result showing the mass losses from the heated-with-flow runs during pre-tests. The slope of the poly-fit line represents to average mass loss rate of 0.020 g/s.

b) Experimental Mass Loss Measurements using Volume-based Method

The measurements with the Romer Multi-Gauge 6 Axis Coordinate Measuring Arm (Part Number: NCA7-05-16186) proved effective in determining the shape of the surface of disc. The measurements were taken along three radii, R1, R2 and R3. Where R1 and R2 were taken along a diameter, and R3 was taken in the direction that is perpendicular to the diameter as shown in Figure 15. An average of nine measurements were taken along each radius.

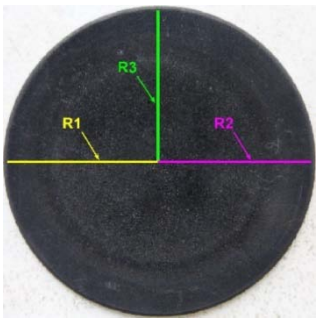

Figure 15: The image of disc was defined by three radii R1, R2 and R3.

Referencing the back surface as facing the plasma and the front surface facing the flow, the thickness of the disc was determined from data obtained on various paths as shown in Figure 16. Disc thickness was defined by the measurements along the three radii on the front of the disc in relation to measurements at the same positions on the backside of the disc. The advantage of using three radii was to get data to identify the precision with which the shape was measured and therefore give data to provide an estimate of the uncertainty with which the shape and mass loss were measured. The measuring arm was only used at the end of the whole series of experiments and not after each run because the required contact to take the measurements would damage the surface and effect the subsequent ablation. Figure 16 shows the relative heights of positions along R1, R2, and R3 at the back and front of the disc. The paths along the back appears to be more consistent when comparing the three radii than the paths along the front. The change in height on the back surface, due to the heating, produces a smoother profile than is evident on the front surface subjected to ablation.

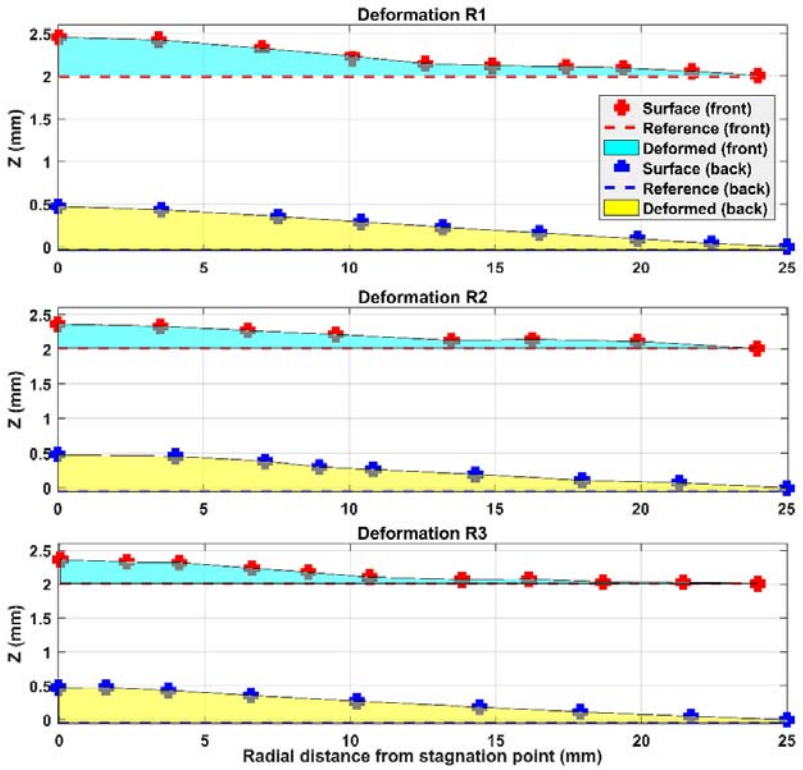

Figure 16: Measurements of the front and back of the disc along paths R1, R2, and R3 after experiments.

Using Figure 16, an average of the thickness at positions along the three radii was calculated and the value was used for calculation of thickness reduction based on an axisymmetric assumption. One end of each radius was the stagnation point; measurements at this common point were necessarily the same. The ends of the radii at the outer edge of the disc were not relative to any particular reference in the raw data taken from the measuring arm. The thickness at these points was obtained from the micrometre measurements and the relative positions along each radius were respectively adjusted. The data in Figure 17 shows the loss in thickness of the disc along R1, R2 and R3. Starting from the edges, the thickness reduction progressively increases to about 12 mm to the stagnation point in the radii direction. The thickness reduction along R1, R2 and R3 was highest between 0 to 12 mm to the stagnation point. The average thickness reduction was about 0.045 mm at the edges and 0.147 mm at the stagnation point. The shaded area shows the profile of material lost from ablation effects. Error bars were calculated using the maximum deviation from an average of data at the various radial positions along the three paths. The data points indicated that there were variations between measurements at the various radial positions along the three radii. The trends are similar along each path, with most deviation from the average occurring in the regions of maximum material loss.

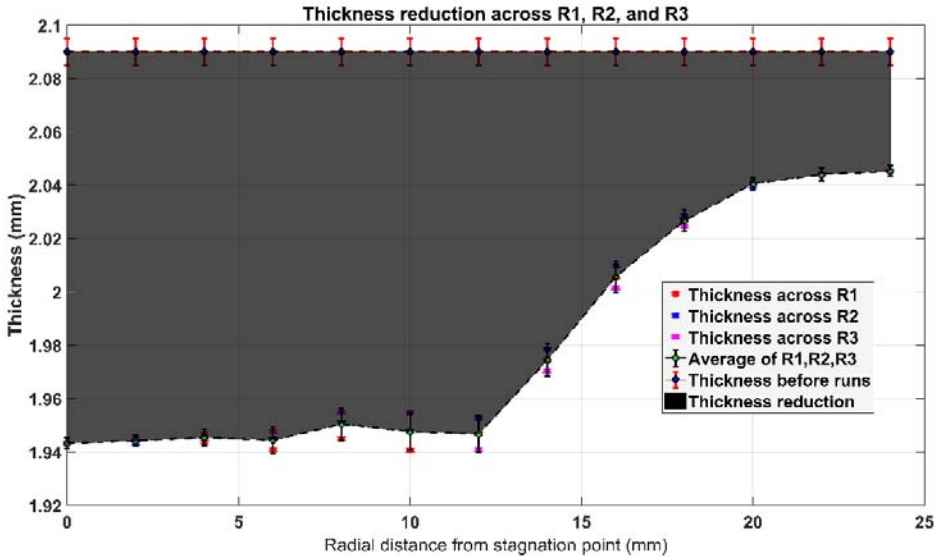

Figure 17: Thickness reduction along paths R1, R2, and R3 after sixteen heated-with-flow experiments.

VI. Surface Roughness of the Disc

The present work does support reasonable contributions to re-entry studies. The experiments show a significant spatial variation in thickness loss for the graphite test material over the disc radius though the spatial variation was still largely axisymmetric. Figure 18 shows the setup for surface analysis using Scanning Electron Microscope (SEM).

(a) SEM arrangement. (b) Disc sample in vacuum chamber.

Figure 18: Setting up and mounting graphite disc in the SEM for surface analysis.

The total area able to be scanned by the SEM was limited: the maximum field of view at the amplification used, was 500 μm. The maximum travel of the specimen holder was 36 mm (18 mm $\times$ 2). Five positions were chosen and used for analysis after each series of runs. The disc was placed in the holder in the same orientation for each set of scans. The centre of the disc was determined by traversing the holder to view the edges of the disc with the y-axis displaced so the extent of travel viewed the edges of the disc, then centring the disc based in these limits. This identified position A in Figure 19 and allowed for 18 mm of travel along the radius of the disc. Five positions in total were chosen at 4.5 mm increments, shown as A, B, C, D, and E in Figure 19. This resulted in position E being 7 mm from the outside edge of the disc (6 mm from the chamfer used to retain the disc).During experiments, the actual points scanned in the SEM were not exactly the same; each scan was a representative area in close proximity to the points described by A, B, C, D and E.

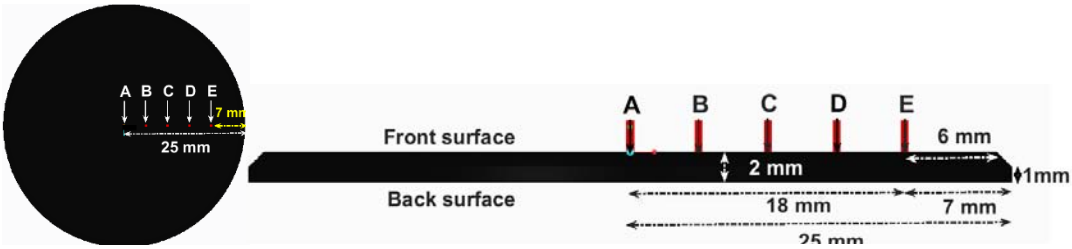

(a) Graphite specimen - top view. (b) Graphite specimen - side view (not to scale).

Figure 19: Schematic illustration of scanning locations on graphite surface.

The SEM system has the capability of producing data which describes the degree of surface roughness. The SEM machine could analyse the relative height across a reference line [Iyinomen 2019]. The SEM data for the surfaces were extracted and plotted as summarised in Figures 20 and 21.

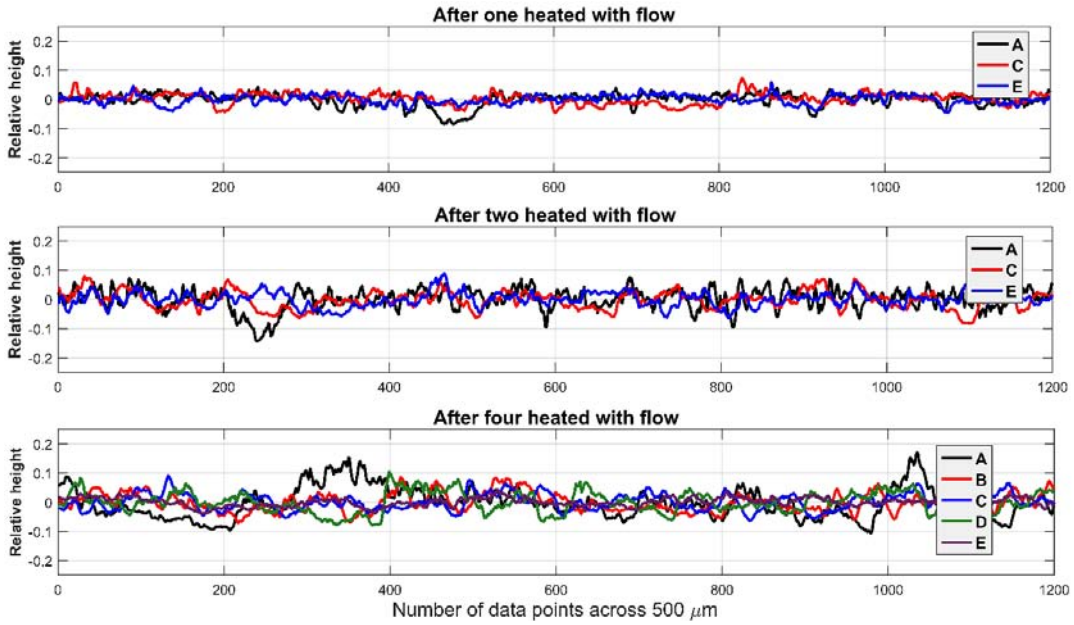

Figure 20: Surface texture relative height summary after 1, 2 and 4 heated-with-flow runs.

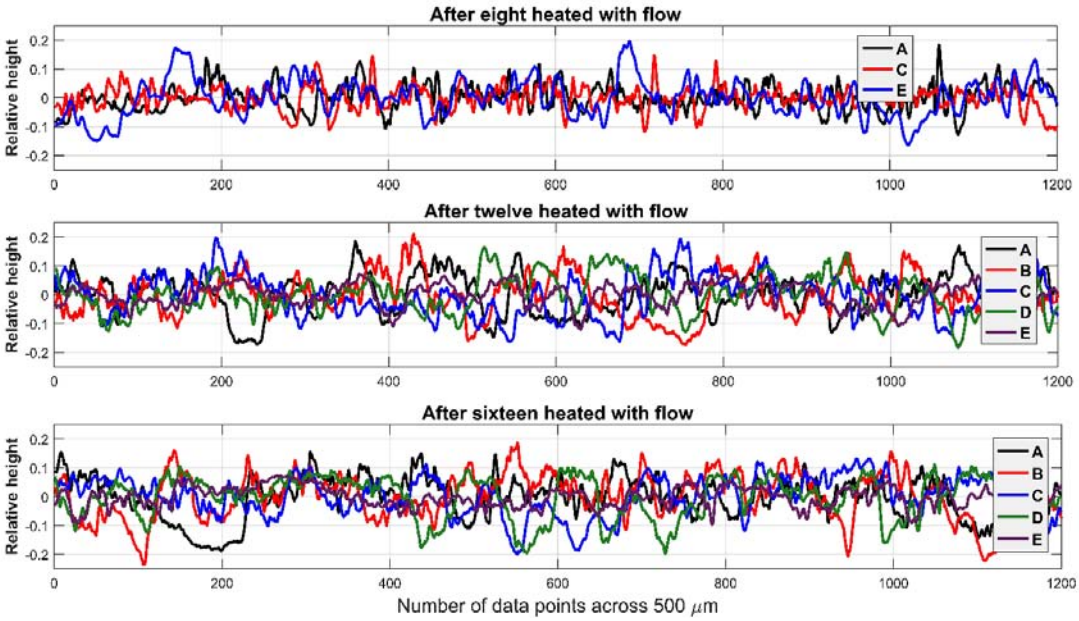

Figure 21: Surface texture relative height summary after 8, 12 and 16 heated-with-flow runs.

Arithmetic average height parameter was used to estimate the surface roughness of the disc. Two basic parameters defining the surface roughness are: (1) maximum height of peaks which defines the maximum height of the profile above the mean line within the assessment length, and (2) maximum depth of valleys which defines the maximum depth of the profile below the mean line within the assessment length [Gadelmawlaet al. 2002]. Determination of roughness using the arithmetic average R_a, defines the deviation of roughness irregularities from the mean line over a sample length n, as shown in Equation 9 [Smith et al. 2003], where y_i is the height at each pixel position along the line profile and $\bar{y}$ is the mean height.

$$R_a = \frac{1}{n}\sum_{i=1}^{n}|y_i - \bar{y}| \qquad \text{Eq. (9)}$$

The degree of surface roughness increases with increasing number of runs, suggesting that potentially larger fragments of carbon are being removed, or the surfaces at the bottom of the valleys are more prone to the ablative actions than those at the peaks. In addition to reducing thickness (increased total material removal), if the increased removal of material from the valleys is occurring, this suggests that chemical reactions are more involved than mechanical erosion. There appears to be a general correlation between the number of runs and the degree of surface roughness as shown in Figure 22. Each point of surface roughness was obtained by averaging the relative heights at each at point C at each SEM measurement. Point C is shown as it is indicative of the ablation changes to the surface involving heating and flow effects. The surface topographies of the disc sample at successive runs for the phase 2 experiments are available in other materials published by the author [Iyinomen 2019, Iyinomen 2022b].

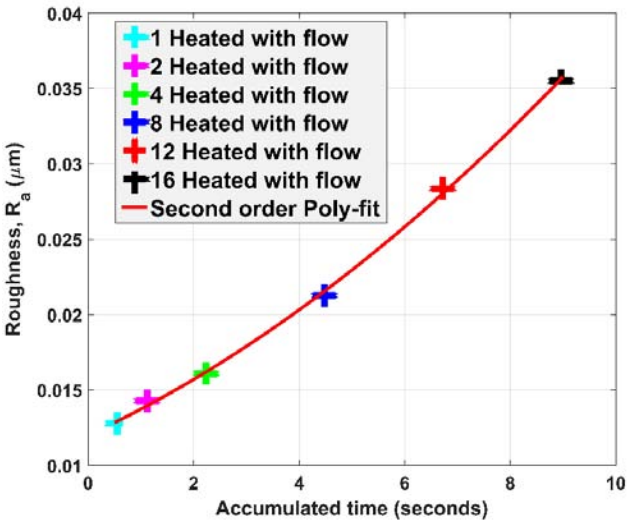

Figure 22: Surface roughness summary from SEM measurements after 1, 2, 4, 8, 12 and 16 heated-with-flow.

VII. Limitations using the Species Spectrometer Measurements

The section does not provide ablation measurement data using species spectrometer but explains why the available spectrometer was not successful for ablation measurements at the time of experiments. Figure 23 shows the experimental setup for ablation experiments using Mach 4.5 nozzle in the blowdown configuration, while Figure 24 shows the analytical CFD and Schlieren imaging from an experimental run.

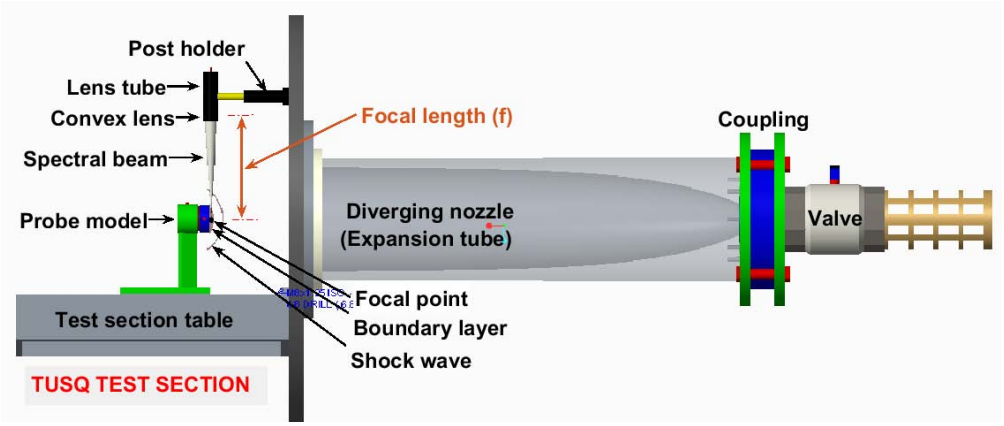

Figure 23: Experimental setup for ablation experiments at Mach 4.5 in the blowdown configuration.

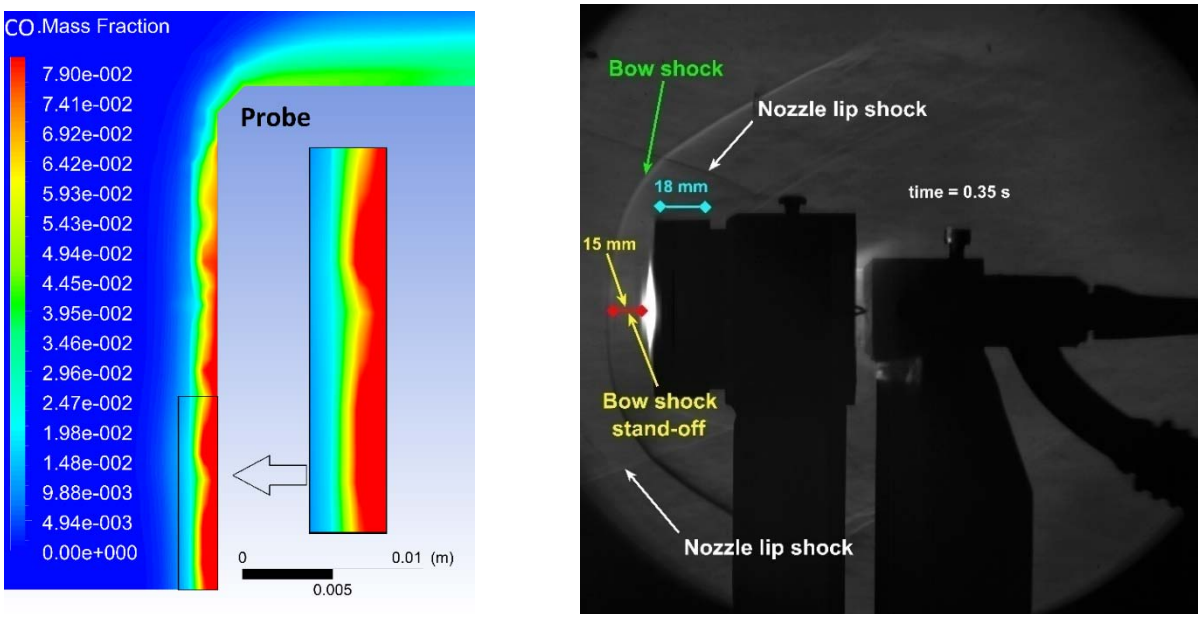

(a) From ablation simulations. (b) From ablation experiments.

Figure 24: Analytical results and experimental run during ablation experiments. The CO_2 mass fraction was about six orders of magnitude lower than that of CO [Iyinomen 2020b].

Figure 25 shows two spectrometers, (1) the Thorlabs CCS175 spectrometer (red) and (2) the Avantes Miniature NIR Spectrometer (blue). The Thorlabs CCS175 spectrometer had a wavelength in the range of 500 - 1000 nm, while the Avantes miniature NIR spectrometer had a wavelength range of 900 - 1750 nm.

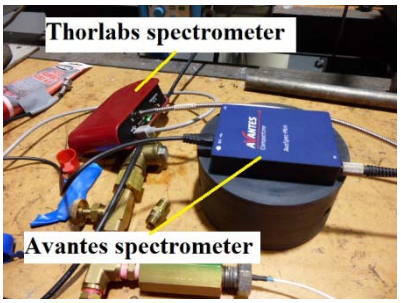

Figure 25: Available species spectrometer at the time of ablation experiments.

Both of them had no moving parts and neither of them could produce good signal for qualitative and quantitative analysis of the surface species. The major reason was because of the background noise. The reacting boundary layer was hot-walled to a cold Mach 4.5 flow. The boundary layer temperature, thickness, species concentrations, type of lens, and potential signal strength were all checked to align with instrumentation and measuring specifications. Figure 26 shows the processed signals from Thorlabs CCS175 spectrometer, while Figure 27 shows the measured and smoothed signals from experiments. These signals were too weak for the author to obtain a high degree of confidence.

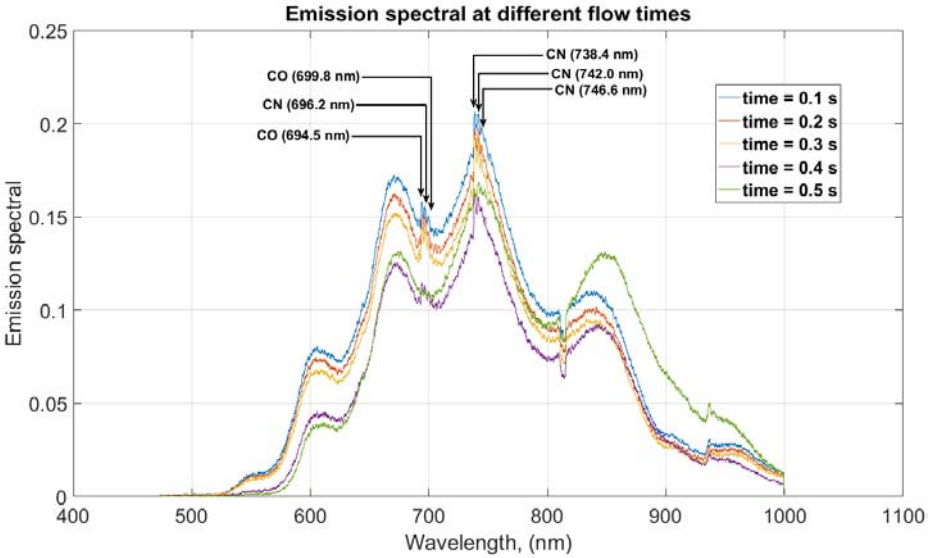

Figure 26: Processed signal from species spectrometer.

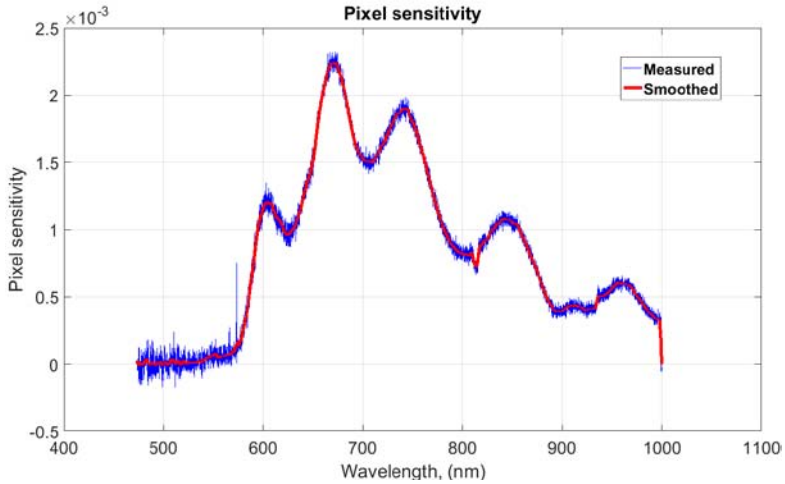

Figure 27: Spectroscopic data showing measured and smoothed signals from experiments.

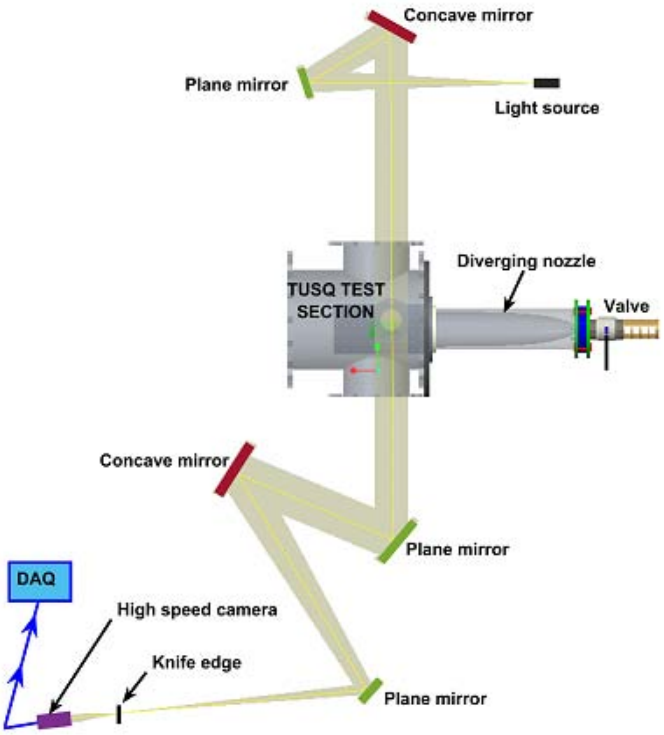

Figure 28: Schematic illustration of the detailed setup for schlieren imaging during experiments.

The author strongly suggests the use of more sophisticated species measuring spectrometers for future experimental programs. The spectrometer should be equipped with liquid nitrogen coolant that will be able to bring the background noise to an acceptable minimum level. This will enable better qualitative and quantitative measurements of ablation species. Also suggested are the use of X-ray Microtomography for spatial microstructural studies, and infrared pyrometers and thermo-cameras to adequately monitor the surface temperature profiles across experimental samples.

VIII. Future Work

Part of the future work will be to use the measurements from present technology to compare with already measured/documented beta-prime for graphite ablation of other researchers, thus creating a good benchmark for verifying the new experimental technique contained herein. There was no evidence of any mass loss on the backside of the graphite sample (where it was heated). This could be as a result of the inert gas (argon) which suppressed the oxygen concentration at the backside [Park 1976] but further investigation needs to be carried out. Also, some aerospace research experts have argued that the application of the new technology to other types of highly porous ablative materials might seem problematic. In the case of graphite, which is regarded as a high thermally conductive material where the heat rapidly distributes over the test sample [Scala and Gilbert 1965], this might not be the case for carbon-phenolics like PICA [Metzger at al 1967], leading to pyrolysis and deformation of the material at the backside [Trick and Saliba 1995] as compared to the frontside within the short time frame. If this happens, the backside would be highly pyrolyzed and ablated [Wong et al. 2015]. Details from oxidation and reaction kinetics [Rosner and Allendorf 1965] from other high enthalpy facilities also need to be compared with the present work.Most newly developed ablators consist of a very porous carbon fibre matrix [Torres-Herrador at al 2021], infiltrated with phenolic resin as decomposing filler (PICA, ASTERM, ZURAM) [Koo and Wang 2022], which have been heavily studied over the past decade [Torres-Herradoret al. 2020]. Such carbon preforms like CBCF 18-2000 can also serve as an ideal candidate for the basic studies of carbon ablation related to thermal heatshields. In order to obtain further thermal distribution parameters that are associated with the new technology, further work needs to be carried out to assess the Biot number using different thicknesses across a range of ablation materials samples. Depending on the wind tunnel facility used, further dimensionless quantities like Re, Ma, Ch, and Da need to be fully characterised with the surface chemistry in order to replicate a specific re-entry trajectory point.

These future works will allow good documentation of any potential drawback(s) that might be associated with the new technology as compared to other facilities.

Using graphite sample, this novel invention has been able to accurately replicate the planetary re-entry surface temperatures and any associated hypersonic flow characteristics within the boundary layer. This patented technological innovation is a new dimension of aerothermodynamics research, fully developed for series of ablation tests in any reliable aerospace laboratory anywhere in the world. To make sure that this innovative technology reaches as many people as possible, the author and his entire research team will continue to be responsible for any unforeseen technical issues. This will help in mutual collaboration by actively supporting aerospace research individuals, centres, agencies, institutions, universities, academia and researchers, thus enabling more re-entry experiments at a minimum cost, without compromising the quality of research outcome. The ongoing continuous improvement of the NGEM will address the structural integrity, by incorporating water cooling system for better survivability in thermally aggressive environments; but again, this depends on the specific need/application. Unlike the present experimental model, the next generation model is simply sophisticated and automated with some C++ programming in the brainbox that made the latest invention to be more versatile for complex re-entry experiments. However, this information remains classified and will barely be made available to the public.

The two major improvements associated the NGEM over the model used in the present work are: (1) a reduction of the heat losses via conduction on the heatshield sample by incorporating a thermal barrier between the test sample and the backshell, and (2) the incorporation of six degrees of freedom (6DOF) to account for variable angle of attacks for better manoeuvrability during re-entry, descent and landing [Iyinomen 2022a]. These increased operational capabilities are the milestone of the NGEM that have never been attempted for any re-entry aerothermodynamics studies elsewhere [Iyinomen 2022a]. The fact that the NGEM is able to attain surface temperatures in excess of 3000 K, will encourage the use of spectroscopic measurements of ablation species and spatial microstructural studies using X-ray Microtomography. Infrared pyrometers and thermo-cameras are also needed to adequately monitor the surface temperature profiles across experimental samples. The aim of the NGEM is to improve the operational capabilities of the new plasma preheating technology by readdressing the thermal and aerodynamic performances of the present work, and the author is doing everything possible to make it happen. These modifications enable the NGEM to be smarter and more practically replicates real-flight vehicles as shown in Figures 29 and 30.

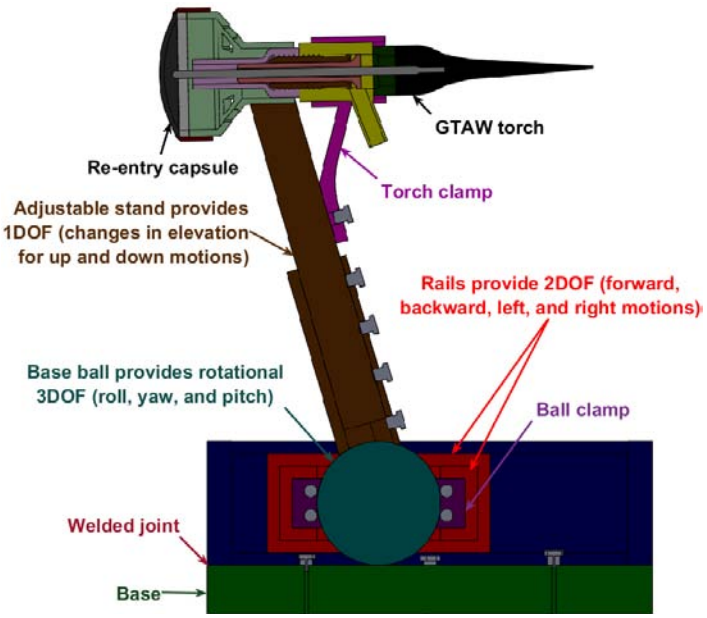

Figure 29: Simplified sectional view showing the improved operational capabilities of the NGEM using an experimental geometric sample of Orion heatshield of 2 mm thickness [Iyinomen 2022a].

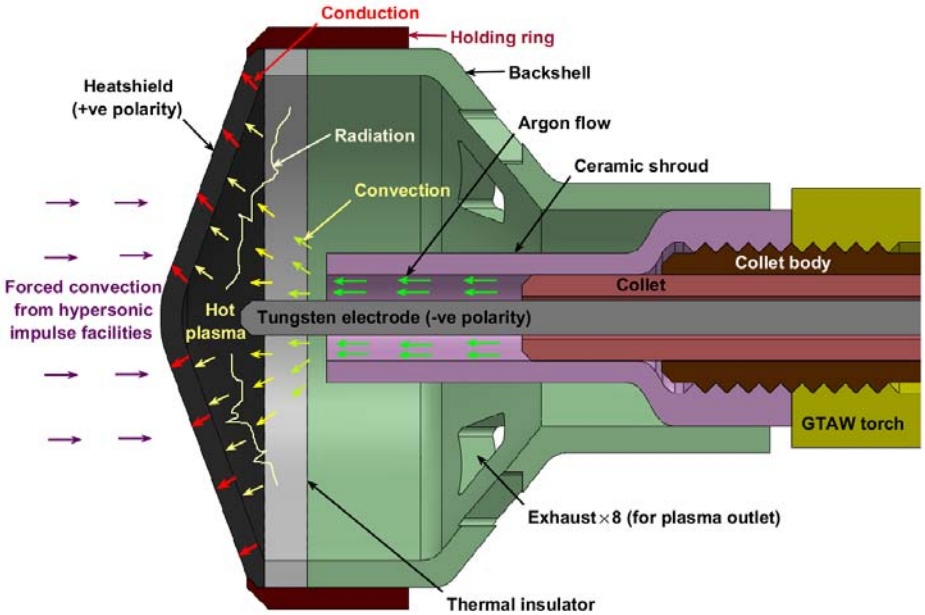

Figure 30: Thermophysics and heat transfer in probe model for future experimental tests using an experimental geometric sample of Stardust heatshield of 2 mm thickness [Iyinomen 2022a].

Table 2: Materials selection for NGEM components and parts to be used for future ablation experiments. The criteria/rationale for the justification of materials selection are contained elsewhere [Iyinomen 2022a].

Component/feature	Present model	NGEM	Scientific relevance
Geometry	Simplified	Advanced	Better operational performance.
Stand	Rigid/fixed	Adjustable	Allows flexibility in elevations
6DOF	Absent	Present	Better aerodynamic manoeuvrability
Backshell	Mild steel	Stainless steel	Housing and support
Backshell thickness	5.0 mm	2.5mm	Reduced mass and heat-sink effects
Holding ring	Mild steel	TiC	Higher thermal capability over steel
Thermal barrier system	Absent	Present	Reduced conduction losses
Ceramic shroud	96% alumina	Zirconia	Higher thermal capability over 96% alumina
GTAW torch	Detached	Attached	Thermal optimisation over detached features

IX. Conclusions

The weighing method concluded that the average mass loss rate was 0.020 g/s for the flow period during sixteen heated-with-flow runs, 0.001 g/s for flow-only and 0.00055 g/s on average for heated-only. Flow-only mass loss rate is about 4.9 % of the average mass loss rate during the flow of heated-with-flow runs. An average mass loss rate during the heated-only runs (and therefore during the heating phase of a heated-with-flow run) is not particularly useful to report. The Scanning Electron Microscope (SEM), the Laser beam visualisations, micrometre gauge, and measurements using the measuring arm were used to identify the shape changes due to ablation. Changing surface characteristics resulting from flow were identified by using the Scanning Electron Microscope (SEM). The results from SEM and laser sheet experiments reveal continuous thickness reduction with increasing number of runs. The major area of interest is using plasma to preheat probe models that can be used for ablation studies in cold-flow hypersonic wind tunnels. The plasma generation is a new technique that generated the needed heat flux for the surface temperature characterisation without using any arc jet or plasmatron facilities. This technique aims to produce a newer and better method of aerothermodynamic tests for investigating ablation samples of re-entry probes in expansion tubes. The probe used was very similar to the European Standard Probe with a stagnation temperature of about 2500 K. This intellectual property is not elsewhere classified and will significantly aid aerothermodynamics of re-entry studies of the entire universe, and provides extremely useful contributions to improving aeroheating test reliability in hypersonic impulse facilities around the world.

Acknowledgments

The author has no connections with the University of Southern Queensland (USQ), where the author carried out an independent research work of the author, by the author, for the author. The author would like to acknowledge his totally 100% self-funded independent PhD student research work, consisting but not limited to 100% payment of all tuition fees, plasma preheating device and accessories costs, experimental consumable costs, analytical costs, transportation costs, living costs, and overseas health insurance costs during his doctoral candidature at USQ. Evidence of financial self-sponsorship and all academic financial statements throughout the full-time doctoral candidature from 2 March 2015 to 13 September 2019 are held at the Graduate Research School of USQ. The author acknowledges the tremendous financial supports that he received from family and friends during difficult times. The author also acknowledges the six (6) times refusal of his student scholarship applications during the doctoral candidature despite high distinctions; but perseverance led to earning a PhD in Mechanical and Aerospace Engineering along with a Doctoral Research Excellence Award for achieving the highest possible result for a Higher Degree by Research thesis examination 2019 at the Institute for Advanced Engineering and Space Sciences, USQ. The author is grateful for the opportunities to continuously exchange professional ideas with his entire research team at Danospace and other aerospace research professionals around the world. The novel preheating technology for ablation experiments reported herein is not elsewhere classified and intellectual property is fully protected by the intellectual property (IP) right of Australia with Patent Number 2019205004.

References Références Referencias

1. Anand, K.R. and Mittal, V., 2017. Review on the parametric optimization of tig welding. International Research Journal of Engineering and Technology (IRJET), Volume: 04 Issue: 01 January 2017 e-ISSN: 2395 -0056, p-ISSN: 2395-0072.
2. Anderson, J.D., 2000. *Hypersonic and high temperature gas dynamics*. AIAA
3. Birch, B., Buttsworth, D., Choudhury, R. and Stern, N., 2018. Characterization of a Ludwieg Tube with Free Piston Compression Heating in Mach 6 Configuration. In 22nd AIAA International Space Planes and Hypersonics Systems and Technologies Conference (p. 5266).
4. Bugel, M., Reynier, P. and Smith, A. Survey of European and major ISC facilities for supporting Mars and sample return mission aerothermodynamics and tests required for thermal protection system and dynamic stability. Int. J. Aerosp. Eng., 2011, 2011. doi: 10.1155/2011/937629.
5. Chhunchha, A.C., 2018. *Aerodynamic Heating Analysis of Re-Entry Space Capsule Using Computational Fluid Dynamics*. California State University, Long Beach.
6. Dec, J. and Braun, R. (2006), An approximate ablative thermal protection system sizing tool for entry system design, in `44th AIAA Aerospace Sciences Meeting and Exhibit', pp. 780-794.
7. Detra, R. W., and Hidalgo, H., 1961, "Generalized Heat Transfer Formulae and Graphs for Nose-Cone Re-Entry into the Atmosphere," ARS Journal, 31, pp. 318-32.
8. Duffa, G., 2013. *Ablative thermal protection systems modeling*. American Institute of Aeronautics and Astronautics, Inc.
9. Fagnani, A., Helber, B. and Chazot, O., 2019, July. Evaluation of Probe-Material Thermal Interaction in Plasma Wind Tunnel Tests by Means of IR Thermography and Thermal Inverse Modelling. In *8th European Conference for Aeronautics and Space Sciences*.
10. Fay, J.A. and Riddell, F.R., 1958. Theory of stagnation point heat transfer in dissociated air. *Journal of the Aerospace Sciences*, *25*(2), pp.73-85.
11. Gadelmawla, E.S., Koura, M.M., Maksoud, T.M.A., Elewa, I.M. and Soliman, H.H., 2002. Roughness parameters. Journal of materials processing Technology, 123(1), pp.133-145.
12. Glass, D. (2008), Ceramic matrix composite (CMC) thermal protection systems (TPS) and hot structures for hypersonic vehicles, in `15th AIAA International Space Planes and Hypersonic Systems and Technologies Conference', pp. 2682-2718.
13. Goulard, R., 1958. On catalytic recombination rates in hypersonic stagnation heat transfer. *Journal of Jet Propulsion*, *28*(11), pp.737-745.
14. Iyinomen, D.O., 2022b. Book Chapter: Plasma Preheating Technology for Ablation Studies of Hypersonic Re-entry Vehicles. *Hypersonic Vehicles - Applications, Recent Advances, & Perspectives*, ISBN 978-1-83969-933-7.
15. Iyinomen D.O., 2022a. Plasma preheating technology for replicating planetary re-entry surface temperatures. The Aeronautical Journal, 126, 297–315. https://doi.org/10.1017/aer.2021.72.
16. Iyinomen, D.O., Malpress, R. & Buttsworth, D., 2021. Technique Development for Investigating Axisymmetric Ablation Models in Hypersonic Impulse Facilities. *AIAA Journal*, *59*(6), pp.1899-1913.
17. Iyinomen, D.O., 2020b. Numerical approach to ablation measurements using a new plasma pre-heating technique. *International Journal of Thermofluids*, *1*, p.100014.

18. Iyinomen, D.O., 2020a. Numerical & experimental analyses of ablation measurements in expansion wind tunnel facilities using a new plasma pre-heating technique. *International Journal of Thermofluids*, *3*, p.100019.
19. Iyinomen, D.O., 2019. Technique development for investigation of axisymmetric graphite sample oxidation in hypersonic flow (Doctoral dissertation, University of Southern Queensland).
20. Julian, H. and Eggers, A.J., 1958. A study of the motion and aerodynamic heating of ballistic missiles entering the earth's atmosphere at high supersonic speeds. *NACA Rept*, *1381*.
21. Koo, J.H. and Wang, J., 2022. Low-density Flexible and Conformal Thermal Protection Systems Materials: A Review. In *AIAA SCITECH 2022 Forum* (p. 1608).
22. Lees, L., 1956. Laminar heat transfer over blunt-nosed bodies at hypersonic flight speeds. *Journal of Jet Propulsion*, *26*(4), pp.259-269.
23. Martin, A., Boyd, I., Cozmuta, I. and Wright, M., 2010, January. Chemistry model for ablating carbon-phenolic material during atmospheric re-entry. In *48th AIAA Aerospace Sciences Meeting Including the New Horizons Forum and Aerospace Exposition* (p. 1175).
24. Metzger, J.W., Engel, M.J. and Diaconis, N.S., 1967. Oxidation and sublimation of graphite in simulated re-entry environments. *AIAA Journal*, *5*(3), pp.451-460.
25. Park, C., 1976. Effects of atomic oxygen on graphite ablation. *AIAA journal*, *14*(11), pp.1640-1642.
26. Poovathingal, S., Schwartzentruber, T.E., Murray, V.J. and Minton, T.K., 2016. Molecular simulation of carbon ablation using beam experiments and resolved microstructure. *AIAA journal*, *54*(3), pp.999-1010.
27. Rosner, D.E. and Allendorf, H.D., 1965. High temperature oxidation of carbon by atomic oxygen. *Carbon*, *3*(2), pp.153-156.
28. Sakraker, I., Chazot, O. and Carvalho, J.P., 2021. Performance of cork-based thermal protection material P50 exposed to air plasma. *CEAS Space Journal*, pp.1-17.
29. Scala, S.M. and Gilbert, L.M., 1965. Sublimation of graphite at hypersonic speeds. *AIAA journal*, *3*(9), pp.1635-1644.
30. Settles, G.S., 2006. High-speed imaging of shock waves, explosions and gunshots: New digital video technology, combined with some classic imaging techniques, reveals shock waves as never before. American Scientist, 94(1), pp.22-31.
31. Siewert, E., Baeva, M. and Uhrlandt, D., 2019. The electric field and voltage of dc tungsten-inert gas arcs and their role in the bidirectional plasma-electrode interaction. Journal of Physics D: Applied Physics, 52(32), p.324006.
32. Smith, J.R., Breakspear, S. and Campbell, S.A., 2003. AFM in surface finishing: Part II. Surface roughness. Transactions of the IMF, 81(3), pp. B55-B58.
33. Sutton, K. and Graves Jr, R.A., 1971. *A general stagnation-point convective heating equation for arbitrary gas mixtures,* NASA Technical Report (No. NASA-TR-R-376).
34. Tauber, M. E., 1989, "A Review of High-Speed Convective Heat Transfer Computation Methods," NASA Technical Report, Paper 2914.
35. Torres-Herrador, F., Eschenbacher, A., Coheur, J., Blondeau, J., Magin, T.E. and Van Geem, K.M., 2021. Decomposition of carbon/phenolic composites for aerospace heatshields: Detailed speciation of phenolic resin pyrolysis products. *Aerospace Science and Technology*, *119*, p.107079.
36. Torres-Herrador, F., Leroy, V., Helber, B., Contat-Rodrigo, L., Lachaud, J. and Magin, T., 2020. Multicomponent pyrolysis model for thermogravimetric analysis of phenolic ablators and lignocellulosic biomass. *AIAA Journal*, *58*(9), pp.4081-4089.
37. Traidia A. 2011, Multi-physics modelling and numerical simulation of GTA weld pools, PhD thesis, Ecole Polytechnique.
38. Tran, H., Johnson, C., Hsu, M.T., Dill, H., Chen-Johnson, A., 2006. Qualification of the forebody heatshield of the Stardust's Sample Return Capsule. In *32nd Thermophysics Conference* (p. 2482).
39. Trick, K.A. and Saliba, T.E., 1995. Mechanisms of the pyrolysis of phenolic resin in a carbon/phenolic composite. *Carbon*, *33*(11), pp.1509-1515.
40. Wang, X., Luo, Y. and Fan, D., 2019. Investigation of heat transfer and fluid flow in high current GTA welding by a unified model. International Journal of Thermal Sciences, 142, pp.20-29.
41. Wong, H.W., Peck, J., Bonomi, R.E., Assif, J., Panerai, F., Reinisch, G., Lachaud, J. and Mansour, N.N., 2015. Quantitative determination of species production from phenol-formaldehyde resin pyrolysis. *Polymer Degradation and Stability*, *112*, pp.122-131.
42. Zhang, K., Bai, S., Zhu, L., Ye, Y., Zhang, H., Ai, Y., Li, S. and Tang, Y., 2019. Ablation and surface heating behaviors of graphite based Ir-Al coating in a plasma wind tunnel. *Surface and Coatings Technology*, *358*, pp.371-377.